Journal of Robotics and Control (JRC)
Volume 6, Issue 3, 2025
ISSN: 2715-5072, DOI: 10.18196/jrc.v6i3.26451

Enhanced Maximum Power Point Tracking for Photovoltaic Systems Using Adaptive Fuzzy Control

Azzeddine Yahia [1*], Mohamed Tahar Makhloufi [2], Kheireddine Chafaa [3], Nadjiba Terki [4], Madina Hamiane [5]
[1, 2, 3] Department of Electronic, University of Batna 2, Batna, Algeria
[4] Laboratory of Vision and Communication Systems, Department of Electrical Engineering, University of Mohamed Khider - Biskra, Algeria
[5] College of Engineering, Royal University for Women, West Riffa 37400, Bahrain
Email: [1] a.yahia@univ-batna2.dz, [2] m.makhloufi@univ-batna2.dz, [3] k.chafaa@univ-batna2.dz, [4] n.terki@univ-biskra.dz, [5] mhamiane@ruw.edu.bh
*Corresponding Author

***Abstract*—The growing need for clean energy has made solar panels an essential solution. However, the nonlinear behavior of photovoltaic (PV) systems under varying weather conditions necessitates advanced control strategies to ensure optimal energy harvesting. This paper presents an enhanced Maximum Power Point Tracking (MPPT) approach that integrates the conventional Perturb and Observe (P&O) method with an Indirect Adaptive Fuzzy Controller (IAFC). While P&O is known for its simplicity, it suffers from steady-state oscillations and slow response during environmental changes. To address these issues, the IAFC adaptively adjusts the perturbation step using a Lyapunov-based rule to improve convergence and minimize power fluctuations. The proposed method achieves Maximum Power Point tracking within less than 0.025 s, compared to 0.05 s for the conventional P&O algorithm. This enhances the credibility of our dynamic performance claim. Specifically, unlike prior fuzzy-P&O hybrids with fixed rule sets, our method leverages Lyapunov-based adaptation to dynamically adjust the control action, improving convergence and robustness under changing conditions. We also included a quantitative metric showing a 75% reduction in power fluctuations compared to conventional P&O. Simulation results under varying sunlight conditions demonstrate fast convergence and improved power stability. The proposed IAFC method clearly outperforms classical P&O in tracking accuracy, responsiveness, and overall energy yield.**

Keywords—Adaptive Fuzzy Control; Lyapunov Stability; Dynamic MPPT Optimization; P&O Improvement; Photovoltaic Systems.

I. INTRODUCTION

Renewable energy systems, such as solar and wind power, are among the most promising sustainable solutions receiving increasing attention in recent research due to their abundance and environmentally friendly nature. These systems contribute significantly to reducing greenhouse gas emissions, making them an effective tool in combating climate change. Additionally, their widespread adoption has been facilitated by declining costs driven by growing global demand [1]-[3].

Among renewable energy sources, solar energy stands out as one of the most widely used and accessible. Photovoltaic (PV) systems convert sunlight directly into electricity through solar cells, offering numerous advantages such as the absence of moving parts, low operational cost, high reliability, and being an inexhaustible energy source [4], [5]. However, the efficiency of PV systems typically ranging between 14% and 19% is greatly affected by environmental factors such as temperature and solar irradiance. These variations introduce nonlinearity in the current-voltage (I-V) and power-voltage (P-V) characteristics of PV modules.

To extract the maximum available power from a PV array, it is crucial to operate the system at the Maximum Power Point (MPP) the point at which the system yields the highest possible output power [6]-[14]. Since the MPP shifts with environmental conditions, especially irradiance and temperature, Maximum Power Point Tracking (MPPT) techniques are essential for maintaining high energy harvesting efficiency [32]-[35].

One of the most widely adopted MPPT techniques is the Perturb and Observe (P&O) method due to its simplicity, ease of implementation, and low cost. This method perturbs the duty cycle of the power converter and observes the resulting change in output power. If the power increases, the perturbation continues in the same direction; otherwise, it is reversed. Despite its effectiveness in steady-state conditions, the P&O technique suffers from limitations such as oscillations around the MPP and degraded performance under rapidly changing environmental conditions. These shortcomings reduce the overall energy extraction efficiency and highlight the need for more advanced and adaptive control strategies [15]-[19].

To address these limitations, various intelligent and adaptive control methods have been introduced, such as Fuzzy Logic Control (FLC). FLC mimics human reasoning and decision-making using linguistic rules and is commonly implemented using Mamdani-type fuzzy sets [20]. This approach is highly effective for handling nonlinear and uncertain systems without requiring precise mathematical modeling, making it suitable for real-world PV applications [21]-[26]. However, FLC systems often face challenges related to high computational load, particularly when dealing

with high-dimensional rule bases, which affects real-time performance.

Another class of advanced control is Adaptive Control, particularly Model Reference Adaptive Control (MRAC). MRAC continuously adjusts controller parameters to ensure the system output follows a predefined reference model, making it robust against dynamic environments and external disturbances. This method has been successfully used in power systems, robotics, and aerospace due to its adaptability and stability based on Lyapunov theory [27]-[31]. Nevertheless, MRAC performance is highly sensitive to inaccuracies in the reference model, which may lead to instability or degraded tracking.

Despite the significant advancements in MPPT strategies, major challenges persist in both fuzzy and adaptive control domains [36]. These include the high computational complexity due to large rule bases (often referred to as the "rule explosion" problem), and the difficulty of real-time parameter tuning during fast environmental changes [37]-[39].

To overcome these challenges, this study proposes a novel hybrid control approach known as Indirect Adaptive Fuzzy Control (IAFC), which synergistically combines the strengths of FLC and MRAC. The IAFC technique leverages the nonlinear handling and uncertainty tolerance of FLC with the adaptive tracking and stability advantages of MRAC. This hybridization not only reduces the required number of fuzzy rules, thus decreasing computational complexity, but also enhances real-time responsiveness compared to other intelligent methods like neuro-fuzzy or metaheuristic-based controllers [55]-[57].

The proposed control system is structured in two levels: in the first level, the conventional P&O technique provides an initial estimation of the optimal duty cycle based on real-time PV voltage and current data. In the second level, the IAFC dynamically fine-tunes the control parameters to ensure stable and accurate MPP tracking under varying environmental conditions.

Simulation results demonstrate that the proposed hybrid approach significantly improves MPPT tracking speed, enhances output power stability, and increases overall energy conversion efficiency compared to traditional techniques, proving its effectiveness in dynamic solar energy applications.

The main contributions of this study are as follows, emphasizing the performance improvements and control robustness achieved:

- Two-Level MPPT Control: A hierarchical control architecture is proposed, where the Perturb and Observe (P&O) method functions as the first-level controller to establish an initial estimate of the optimal duty cycle based on real-time PV voltage and current measurements.
- Enhanced Dynamic Response: The second-level controller, based on IAFC, adaptively fine-tunes the control parameters in response to rapid environmental fluctuations, thereby maintaining efficient tracking of the Maximum Power Point (MPP) under dynamic conditions.
- Optimized Power Conversion Efficiency: The hybrid P&O-IAFC structure achieves superior energy harvesting by improving tracking precision and ensuring stable and adaptive regulation of the DC-DC power converter.
- Comprehensive Performance Assessment: The proposed control strategy is validated through comparative simulations against the conventional P&O method. Results demonstrate clear improvements in tracking speed, output power stability, and overall energy conversion efficiency.

The structure of this paper is organized as follows to provide a clear and comprehensive understanding of the proposed work. Section 2 presents the modeling of the solar energy conversion system, including the photovoltaic (PV) array, MPPT controller, and DC-DC power converter. Section 3 introduces the proposed enhanced two-level Maximum Power Point Tracking (MPPT) control scheme, detailing its implementation and advantages. Section 4 discusses the research findings obtained from simulations, analyzing the performance of the proposed approach under different conditions. Finally, Section 5 provides conclusions on the effectiveness of the proposed method and outlines potential directions for future research.

II. DESCRIPTION OF THE SOLAR ENERGY CONVERSION SYSTEM

Photovoltaic energy has gained increasing attention in electrical power applications due to its status as a nearly limitless and widely accessible energy resource. However, the power output from photovoltaic (PV) modules depends on factors such as solar irradiance and the temperature of the solar cells. To optimize the efficiency of a solar energy conversion system shown in Fig. 1, it is crucial to track the PV array's maximum power point (MPP). The MPP is a unique point at which the PV array can deliver maximum power to the load. This point, however, changes nonlinearly with variations in solar irradiance and cell temperature. To ensure an optimal operation of the PV array at its MPP, the system needs to include a maximum power point tracking (MPPT) controller. A key component in the solar energy conversion process is the power converter, which converts the direct current (DC) generated by the solar panels into usable voltage and current for the load. When combined with an MPPT algorithm, this power boost converter enables the load to operate at maximum power. The MPPT control algorithm adjusts the operating point of the solar panels in real time to maximize the energy harvested, even in presence of fluctuations in temperature and sunlight. This process ensures that the solar system operates with maximum efficiency, making the best possible use of the generated energy. In this work, a DC-DC power converter is implemented [40].

A. Model and Characteristics of the Photovoltaic (PV) System

The components of a standard photovoltaic (PV) cell configuration are a current source, a diode, and a number of resistors coupled in series and parallel. Fig. 2 depicts the analogous circuit for the PV cell. The current-voltage (I-V)

and power-voltage (P-V) characteristics for varying solar irradiance are depicted in Fig. 3.

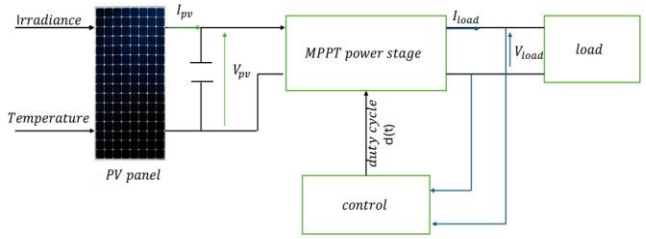

Fig. 1. Solar energy conversion system

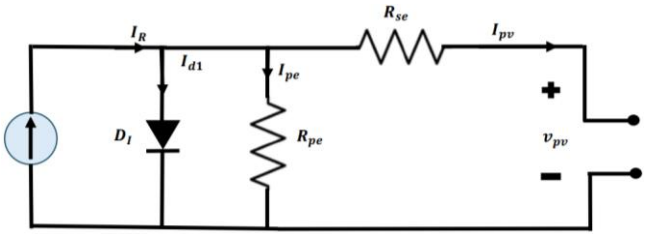

Fig. 2. PV system equivalent circuit

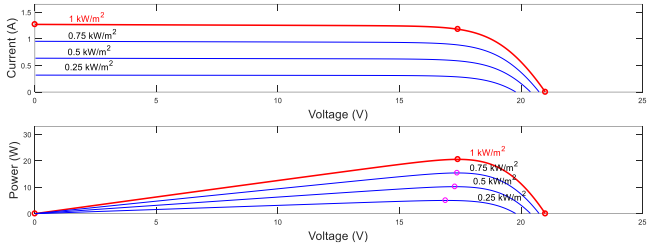

Fig. 3. I-V and P-V curves of the PV system under various levels of solar irradiance

The current produced by a solar cell can be determined using the following equations [2]:

$$i_{pv} = I_R - I_{d1} - I_{pe} \quad (1)$$

In the context of a PV array, the output current and voltage are represented by i_{pv} and v_{pv} respectively. In Equation (1), I_R , I_{pe} and I_{d1} denote the PV cell, the parallel resistanceR_{pe} and diode currents respectively. The diode current I_{d1} is given by:

$$I_{d1} = I_{01}\left(e^{q\frac{(v_{pv}+i_{pv}R_{se})}{nkT}} - 1\right) \quad (2)$$

Where T, q, K, and n stand for temperature, electron charge, Boltzmann's constant, and diode factor, respectively, and I_{01} for reverse saturation current. The following formula can be used to calculate the PV cell current I_R:

$$I_R = \frac{W}{W_0}\left(I_C + \lambda(T - T_0)\right) \quad (3)$$

Where I_c, which represents the short circuit current, is dependent on the irradiance (W) and reference irradiance W_0 during the day, as well as the temperature (T) and reference temperature (T_0). Additionally, I_c is also influenced by the temperature coefficient, λ Equation 4 gives the solar cell output current.

$$I_{pv} = I_R - I_{01}\left(e^{q\frac{(v_{pv}+i_{pv}R_{se})}{nkT}} - 1\right) - \frac{v_{pv} + i_{pv}R_{se}}{R_{pe}} \quad (4)$$

Where R_{se} denotes the series resistance and I_{01} is defined as follows:

$$I_{01} = I_{01ref}\left(\frac{T}{T_0}\right)^3 e^{\left[\frac{qE_G}{nk}\left(\frac{1}{T}-\frac{1}{T_0}\right)\right]} \quad (5)$$

With E_G referring *to the energy bandgap.*

B. Dynamic Model of the Boost Converter

In a simple PV system with single level MPPT control, the steady-state relationship between the PV array voltage (V_{pv}), PV array current (I_{pv}), and the duty cycle (d) of the switching transistor (Q) can be written as follows [41]:

$$v_{pv} = i_{pv}R_0(1 - d)^2 \quad (6)$$

Where v_{pv}, i_{pv} are the PV array voltage and current averages in DC terms. $\hat{v}_{pv}, \hat{\imath}_{pv}$ are the ripple terms, and Ro is the load resistance.

The relationship (6) forms the basis for conventional MPPT algorithms, which calculate the converter's duty cycle during steady states. However, to optimize transient responses, MPPT control must consider the dynamic interaction between the duty cycle and the array voltage. Undesirable transient oscillations can occur, potentially leading to inefficient system operation. Therefore, the MPPT control mechanism must eliminate these transient oscillations in array voltage once the duty cycle has been adjusted to accommodate changing environmental conditions. A comprehensive dynamic model of the boost converter is proposed in [42]. To simplify the analysis of the system's transient response, a small signal equivalent circuit is adopted, as proposed in [43]. The circuit is shown in Fig. 4.

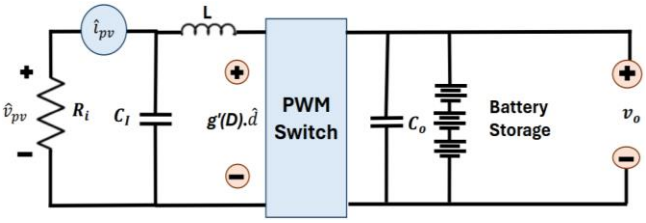

Fig. 4. Small signal equivalent circuit for PV array and boost converter

The PV array with small-signal array voltage $\hat{v}_{pv}$ and small-signal array current $\hat{\imath}_{pv}$ is represented by the resistance R_i in the circuit. The transfer function (TF) is established between the duty cycle control signal d(t) and the voltage across the array v_{pv} (t) at a specific operating point. The system's dynamics are encapsulated within this TF. Fig. 4 depicts a dynamic model with a battery load commonly found in PV systems. In this context, the TF between the duty cycle and the array voltage is derived under small signal operation, disregarding the battery dynamics. Through the analysis of Fig. 4, we derive the following correlation [44].

$$\frac{\hat{v}_{pv}(s)}{R_i} + s\hat{v}_{pv}(s)c_I = \frac{\acute{g}(D)\hat{d}(s) - \hat{v}_{pv}(s)}{sL} \quad (7)$$

where $\hat{d}(s)$ represents the small-signal variation around the converter's duty cycle D. The relationship between v_{pv} and D is denoted by g(D), and its derivative with respect to D is represented as g′(D).

Drawing from Equation (7), we derive the following expression for the transfer function:

$$\frac{\hat{v}_{pv}(s)}{\hat{d}(s)} = \frac{\acute{g}(D)}{LC_I s^2 + \frac{1}{R_i}s + 1} \quad (8)$$

The Laplace transforms of $\hat{v}_{pv}(t)$ and $\hat{d}(t)$ are denoted by $\hat{v}_{pv}(s)$ and $\hat{d}(s)$ respectively. The boost converter's steady-state output voltage v_0, steady-state DC PV array voltage v_{pv}, and running duty cycle D are related by the function g(D), which may be expressed as [45].

$$g(D) = v_{pv} = (1 - D)v_0 \quad (9)$$

Assuming that that g(D) and v_0 are not affected by transient switching behavior Equation (9) gives $\acute{g}(D) = -v_0$ Therefore, the transfer function in Equation (8) can be re-written as:

$$\frac{\hat{v}_{pv}(s)}{\hat{d}(s)} = \frac{-\frac{v_0}{LC_I}}{s^2 + \frac{1}{R_i C_I}s + \frac{1}{LC_I}} \quad (10)$$

The equation (10) represents the small-signal transfer function used to describe the output voltage dynamics of the boost converter.

This second-order system represents the relationship between duty cycle perturbation $\hat{d}(s)$ and output voltage $\hat{v}_{pv}(s)$, under the assumption of ideal components. The model captures the dominant dynamics of the boost converter using the inductor L, input capacitorC_I, and load resistance R_i, which are sufficient for initial controller design and stability analysis [63].

While parasitic elements such as equivalent series resistance (ESR) of the capacitor, inductor resistance, and switch/conduction losses are neglected, this simplification is widely adopted in control-oriented modeling. Including these losses would result in a more complex higher-order model, making analytical derivation of control laws (such as the MRAC-based adaptation) significantly more cumbersome. However, it is acknowledged that parasitic effects can impact steady-state efficiency and transient behavior, especially under high-frequency switching [64].

Considering the negative sign in the transfer function (10), which suggests that an increase in PV panel voltage happens when the duty ratio is decreased, and considering that parasitic power stage components were excluded from the analysis, the transfer function is determined for a nonlinear system as depicted in Fig. 3 near a single operating point using its linearized version as illustrated in Fig. 4 [2].

III. MPPT CONTROLLER DESIGN

The enhanced 2-level Maximum Power Point Tracking (MPPT) control scheme proposed in this work is designed to efficiently track the Maximum Power Point (MPP) amidst varying environmental conditions. The operating point is adjusted to the ideal value of the resistance R using the perturb and observe first level of control [46]. The novel IAFC controller, which regulates the converter dynamics at the second level of control, makes sure that the ideal resistance (R) produces a critically damped system response even in the face of changing environmental conditions. Similar to Ripple Correlation Control (RCC), which use ripple in PV voltage to accomplish MPPT, the adaption gain of the IAFC is modified based on the high-frequency (ripple) content of the tracking error. [52] This high-frequency content of the tracking error accurately reflects variations in input parameters. Consequently, the adaptation gain of the IAFC is tuned more effectively to address the impact of changing environmental conditions on the PV system's output voltage. This guarantees rapid convergence, enhances transient performance, and avoids the need for excessively high adaptation gain while ensuring the absence of high-frequency oscillations in the control signal. A comprehensive methodology detailing the proposed approach is provided in the subsequent section. The novelty of the proposed IAFC controller lies in its Lyapunov-guided adaptation, which ensures closed-loop stability without requiring prior knowledge of nonlinear functions f(x) and g(x). This distinguishes it from conventional FLC or MRAC schemes, which typically assume fixed rules or accurate plant models [58].

A. *Perturb and Observe Methode (First Control Level)*

At the first level, the perturb and observe method is used to calculate the duty cycle d(t) in order to deliver maximum power in steady state. This calculated duty cycle d(t) serves as an input for the proposed novel IAFC unit. The general schematic architecture of the recommended control strategy is illustrated in Fig. 5. The MPPT control law is expressed in Equation (11).

$$\frac{dp}{dv_{pv}} = \begin{cases} = 0, at\ MPP \\ > 0, at\ left\ side\ of\ MPP \\ < 0, at\ right\ side\ of\ MPP \end{cases} \quad (11)$$

The flowchart for the calculation block d(t) = r of the suggested MPPT approach is portrayed in Fig. 6.

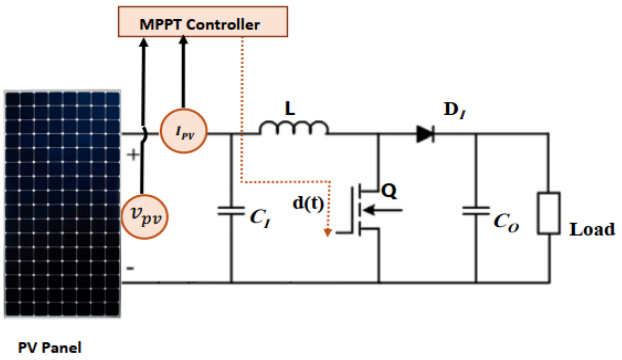

Fig. 5. PV system with boost converter and MPPT controller

B. *Proposed Indirect Adaptive Type 1 Fuzzy Controller Method (Second Control Level)*

The design of the proposed secondary control level, namely IAFC, is depicted in Fig. 7. The IAFC obtains its reference signal d(t) = r from the disturbance and monitoring

unit. The primary objective of the IAFC is to enhance transient performance in Maximum Power Point Tracking (MPPT) by addressing the rapid dynamics of nonlinear PV systems in varying environmental conditions, all without the necessity for consistently high adaptive gain. In the initial stage of the proposed MPPT control, the Disturbance and Monitoring unit analyzes high-frequency components and aligns them with the switching function to guide the control process [47].

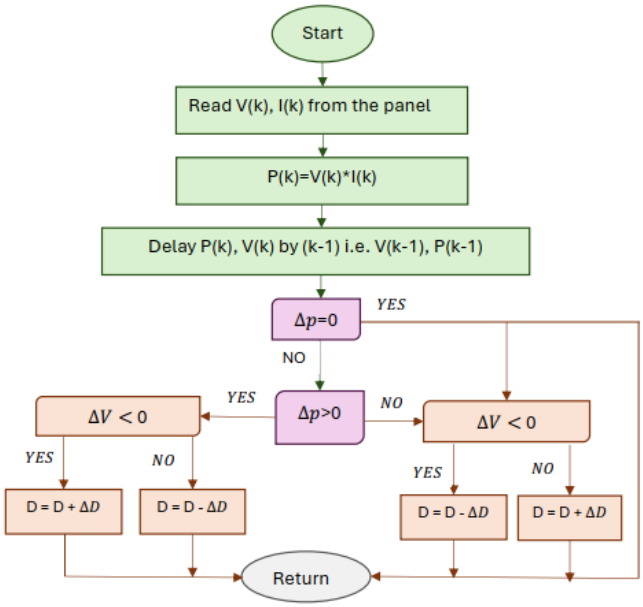

Fig. 6. Flowchart of perturb and observe algorithm

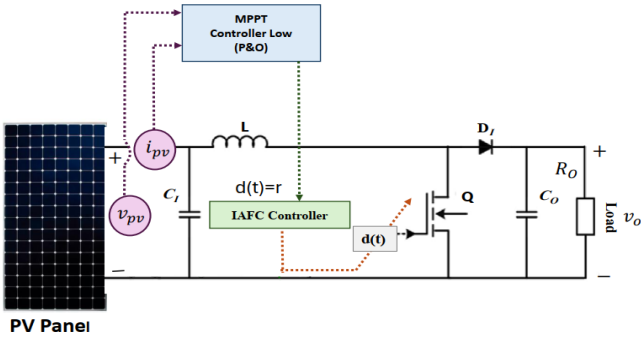

Fig. 7. Adaptive MPPT controller for photovoltaic systems

1) *Reference and Plant Model*

Equation (10) represents the plant model for the proposed IAFC using positive coefficients in both time and frequency domain formulations.

$$\frac{d^2y_p(t)}{dt^2} = -a_p\frac{dy_p(t)}{dt} - b_p y_p(t) + k_p u_p(t) \tag{12}$$

$$G_p(s) = \frac{y_p(s)}{u_p(s)} = \frac{k_p}{s^2 + a_p s + b_p} \tag{13}$$

Where a_p, b_p *and* k_p are the plant parameters and can be expressed in terms of the PV system parameters from equation (10).

The second-order reference model has been selected, both in the time and frequency domains, to represent the desired output $y_m(t)$ for the input $r(t)$ with the following form:

$$\frac{d^2y_m(t)}{dt^2} = -a_m\frac{dy_m(t)}{dt} - b_m y_m(t) + k_m r(t) \tag{14}$$

$$G_m(s) = \frac{y_m(s)}{r(s)} = \frac{k_m}{s^2 + a_m s + b_m} \tag{15}$$

Where k_m is a positive gain, $a_m$and $b_m$are calculated such that the reference model generates a critically damped step response. The purpose of the control strategy is to adjust u(t) so that $y_p(t)$ asymptotically follows $y_m(t)$.

The following subsections explore the controller design and state-space analysis to develop an error-dependent adjustable gain strategy aimed at improving the transient response in the 2-level MPPT control.

2) *Probleme Formulation*

Consider a nonlinear system of order n defined by:

$$\begin{aligned} \dot{x}_1 &= x_2 \\ \dot{x}_2 &= x_3 \\ &\vdots \\ \dot{x}_n &= f(x_1, x_2, \dots, x_n) + g(x_1, x_2, \dots, x_n)u \end{aligned} \quad y = x_1 \tag{16}$$

which is equivalent to:

$$x^{(n)} = f\left(x, \dot{x}, \dots, x^{(n-1)}\right) + g\left(x, \dot{x}, \dots, x^{(n-1)}\right)u \tag{17}$$

Let f and g be unknown continuous functions, where $u \epsilon R$ *and* $y \epsilon R$ are the input and output of the system respectively. The state vector of the system is denoted as $\underline{x} = (x_1, x_2, \dots\ x_n)^T = \left(x, \dot{x}, \dots, x^{(n-1)}\right)\epsilon R^n$. For the system (17) to be controllable, it is required that $g\left(\underline{x}\right) \neq 0$ for x belonging to a certain controllability region $u_c \subset R^n$. Since g(x) is continuous, it is assumed that $g\left(\underline{x}\right) > 0\ \forall \underline{x}\epsilon u_c$.

The objective of the control strategy is to force y to track a predefined reference signal $y_m(t)$.while making sure that all involved signals remain bounded. Specifically, the aim is to determine a control law $u = u(\underline{x}/\theta)$ based on a type 1 fuzzy system, along with an adaptive law for adjusting the parameter vector θ. This is accomplished through the following:

1. It is essential for the closed-loop system to exhibit global stability, ensuring that all variables $\underline{x}(t), \underline{\theta}(t)$ *and* $u(\underline{x}/\theta)$ remain uniformly bounded. In other words, the aim is to ensure that $\left|\underline{x}(t)\right| \leq M_x < \infty, \left|\underline{\theta}(t)\right| \leq M_\theta < \infty$ *and* $u(\underline{x}/\theta) \leq M_u < \infty$ for all $t \geq 0, where M_x, M_\theta and\ M_u$ represent design parameters defined by the designer.
2. The tracking error, denoted as $e = y_m - y$, should be minimized and tend towards zero. If the functions f and g were given, the control law would be determined as follows: $\underline{e} = \left(e, \dot{e}, \dots, e^{(n-1)}\right)^T and\ \underline{k} = (k_n, \dots, k_1)^T where\ k \in R^n$ considering such that all the poles of the polynomial $h(s) = s^n + k_1 s^{(n-1)} + \cdots + k_n$ are situated in the open left half-plane.

$$u = u\left(\underline{x}\right) = \frac{1}{g\left(\underline{x}\right)}\left[-f\left(\underline{x}\right) + {y_m}^{(n)}(t) + \underline{k}^T\underline{e}\right] \tag{18}$$

This allows for the derivation of the error dynamics as follows.

$$e^{(n)} + k_1 e^{(n-1)} + \cdots + k_n e = 0 \tag{19}$$

and since the polynomial h(s) is stable, then $e(t) \to 0$ which is the main objective of the control.

a) Indirect Type 1 Fuzzy Controller

In practice, since f and g are unknown, they must be substituted with their estimations $\hat{f} and\ \hat{g}$, which will be type-1 fuzzy systems. As a result, the new control law will adopt the following form.

$$u_c = u_c(\underline{x}/\underline{\theta}_f, \underline{\theta}_f)\frac{1}{\hat{g}(\underline{x}/\underline{\theta}_g)}\left[-\hat{f}(\underline{x}/\underline{\theta}_f) + y_m{}^{(n)}(t) + \underline{k}^T\underline{e}\right] \tag{20}$$

Applying equation (20) to equation (17) and conducting some manipulations, the following error equation is obtained:

$$\begin{aligned} e^n = -\underline{k}^T\underline{e} + \left[\hat{f}(\underline{x}/\underline{\theta}_f) - f(\underline{x})\right] \\ + \left[\hat{g}(\underline{x}/\underline{\theta}_g) - g(\underline{x})\right] u_c \end{aligned} \tag{21}$$

This is equivalent in state-space formulation to the following.

$$\dot{\underline{e}} = A_c\underline{e} + \underline{b_c}\left[\left(\hat{f}(\underline{x}/\underline{\theta}_f) - f(\underline{x})\right) + \left(\hat{g}(\underline{x}/\underline{\theta}_g) - g(\underline{x})\right)u_c\right] \tag{22}$$

Where

$$A_c = \begin{bmatrix} 0 & 1 & 0 & 0 & \dots & 0 & 0 \\ 0 & 0 & 1 & 0 & \dots & 0 & 0 \\ \dots & \dots & \dots & \dots & \dots & \dots & \dots \\ 0 & 0 & 0 & 0 & \dots & 0 & 1 \\ -k_n & -k_{n-1} & \dots & \dots & \dots & \dots & -k_1 \end{bmatrix}. b_c = \begin{bmatrix} 0 \\ \dots \\ 0 \\ 1 \end{bmatrix} \tag{23}$$

which can be rephrased as follows: Since matrix A_c is stable, implying that the characteristic polynomial $\left(|sI - A_c| = s^n + k_1 s^{(n-1)} + \cdots + k_n\right)$ has all its roots in the open left-half complex plane (i.e., they have negative real parts), then , there exists a symmetric positive definite matrix P of order $(n \times n)$ which satisfies the Lyapunov equation,

$$A_c^T + PA_c = -Q \tag{24}$$

Given that Q is an arbitrary positive definite matrix of order $n \times n$, and $A_c$the closed-loop system matrix. Lyapunov's direct method was employed to ensure the global asymptotic stability of the closed-loop system. The candidate Lyapunov function used is, [48], [49]:

$V_e = \frac{1}{2}\underline{e}^T P\underline{e}$,where e is the tracking error between the actual system output and the reference model. The time derivative of the Lyapunov function is $\dot{V}(e) = e^T P\dot{e} = -\frac{1}{2}\underline{e}^T Q\underline{e} \le 0$ This condition ensures that the error $e(t) \to 0\ as\ t \to \infty\ \infty$ thus proving global asymptotic stability.

Furthermore, the adaptive laws for the fuzzy parameters were derived based on Lyapunov's method to ensure convergence while keeping the parameter estimates bounded.

The Lyapunov-based stability analysis presented in Eq. (24), namely, serves as a theoretical guarantee for the asymptotic stability of the closed-loop system under the proposed IAFC scheme. This formulation ensures that the chosen adaptation law drives the tracking error to zero, provided that the system parameters remain within the assumed nominal bounds. However, we acknowledge that real-world systems are subject to parameter variations and uncertainties particularly in photovoltaic systems where irradiance, temperature, and component tolerances can vary significantly. While the theoretical analysis guarantees nominal stability, we agree that a sensitivity analysis would provide deeper insight into the robustness of the proposed controller [59]-[62]. So, using equations (22) and (24) we obtain.

$$\begin{aligned} \dot{V}_e = \frac{1}{2}\dot{\underline{e}}^T P\underline{e} + \frac{1}{2}\underline{e}^T P\dot{\underline{e}} \\ = -\frac{1}{2}\underline{e}^T Q\underline{e} \\ + \underline{e}^T P\underline{b_c}\left[\left(\hat{f}(\underline{x}/\underline{\theta}_f) - f(\underline{x})\right)\right. \\ \left. + \left(\hat{g}(\underline{x}/\underline{\theta}_g) - g(\underline{x})\right)u_c\right] \end{aligned} \tag{25}$$

To ensure that $x_i = y_m^{(i-1)} - e^{(i-1)}$ remains bounded, it is necessary for V_e to be bounded as well. This requirement is equivalent to having $\dot{V}_e \le 0$ when V_e exceeds a certain constant $\widetilde{V}$. From equation (25), we observe that finding u_c such that the last term of (25) is negative seems challenging. To address this issue, the supervision command needs to be invoked.

b) Supervisory Controller

To resolve the issue mentioned in the preceding paragraph, a control term u_s is added to u_c This leads to the following command law.

$$u = u_c + u_s \tag{26}$$

The extra control term u_s is referred to as the supervision command. Its purpose is to ensure that $\dot{V}_e \le 0$ when $V_e > \tilde{V}$ By substituting equation (26) into (17) and performing similar manipulations as those used to derive (22), the following revised error equation is obtained:

$$\begin{aligned} \dot{\underline{e}} = A_c\underline{e} + \underline{b_c}\left[\left(\hat{f}(\underline{x}/\underline{\theta}_f) - f(\underline{x})\right)\right. \\ + \left(\hat{g}(\underline{x}/\underline{\theta}_g) - g(\underline{x})\right)u_c \\ \left. - g(\underline{x})u_s\right] \end{aligned} \tag{27}$$

Using (27) and (24), we get:

$$\begin{aligned} \dot{V}_e = -\frac{1}{2}\underline{e}^T Q\underline{e} + \underline{e}^T P\underline{b_c}\left[\left(\hat{f}(\underline{x}/\underline{\theta}_f) - f(\underline{x})\right)\right. \\ + \left(\hat{g}(\underline{x}/\underline{\theta}_g) - g(\underline{x})\right)u_c \\ \left. - g(\underline{x})u_s\right] \\ \le -\frac{1}{2}\underline{e}^T Q\underline{e} + \left|\underline{e}^T P\underline{b_c}\right|\left[\left|\hat{f}(\underline{x}/\underline{\theta}_f)\right| + \left|f(\underline{x})\right|\right. \\ \left. + \left|\hat{g}(\underline{x}/\underline{\theta}_g)u_c\right| + \left|g(\underline{x})u_c\right|\right] \\ - \underline{e}^T P\underline{b_c}g(\underline{x})u_s \end{aligned} \tag{28}$$

The constraints of $f\ and\ g$ must be understood in order to formulate u_s so that the right-hand side of e Equation (28) is non-positive. The following presumptions will therefore be made:

Assumption 1:

The functions $f^u(\underline{x}), g^u(\underline{x})\ and\ g_L(\underline{x})\ such\ as\ f|(\underline{x})| \le f^u(\underline{x})\ and\ g_L(\underline{x}) \le g(\underline{x}) \le g^u(\underline{x})\ with\ f^u(\underline{x}) < \infty, g^u(\underline{x}) < \infty\ and\ g_L(\underline{x}) > 0 \forall\ \underline{x} \in U_c$ can be determined mathematically. Due to this assumption, the system (17) can be regarded as partially known rather than completely unknown.

Given $f^u, g^u and\ g_L$ considering equation (28), u_s can be selected as follows: [50]

$$u_s = I * sgn\left(\underline{e}^T P \underline{b}_c\right)\frac{1}{g_L(\underline{x})}\left[\left|\hat{f}(\underline{x}/\underline{\theta}_f)\right| + f^u(\underline{x}) + \left|\hat{g}(\underline{x}/\underline{\theta}_g)u_c\right| + \left|g^u(\underline{x}/\underline{\theta}_g)u_c\right|\right] \quad (29)$$

In Eq. (29), the terms $g_L\ and\ g_u$ represent the known lower and upper bounds of the uncertain nonlinear function g(x), respectively. These bounds are used to ensure that the adaptation law operates within a predefined safe range. To enhance clarity and consistency, we have revised the notation and explicitly stated in the manuscript that $g_L \le g(\underline{x}) \le g_u$where both $g_L\ and\ g_u$ are constant scalars derived from empirical observations of system behavior.

Where $I^* = 1\ if\ V_e > \tilde{V}\ and\ I^* = 0\ if\ V_e \le \tilde{V}$ Substituting (29) into (28) and consolidating the case where, $I^* = 1$ we get:

$$\dot{V}_e \le -\frac{1}{2}\underline{e}^T Q \underline{e} + \left|\underline{e}^T P \underline{b}_c\right|\left[\left|\hat{f}\right| + |f| + |\hat{g}u_c| + |gu_c|\right] - \frac{g}{g_L}\left[\left|\hat{f}\right| + f^u + |\hat{g}u_c| + |g^u u_c|\right] \le -\frac{1}{2}\underline{e}^T Q \underline{e} \le 0 \quad (30)$$

In summary, employing the control action of command (26) with u_c given by (20), we can ensure that $V_e \le \tilde{V} < \infty$. Given that P is positive definite, the constraint on V_e implies a constraint $\underline{e}$ ensuring that $\underline{x}$ remains bounded. It is worth noting that all quantities in (20) and (29) are measurable. Consequently, the control law (26) is implementable.

From Equation (29) It is observed that u_s is non-zero only when the error function V_e exceeds a positive constant $\tilde{V}$. If the closed-loop system under the fuzzy controller u_c operates effectively, implying low error($V_e \le \tilde{V}$), then the supervision command u_s remains zero. Conversely, if the system tends toward instability $(V_e > \tilde{V}), u_s$begins to intervene to enforce $V_e \le \tilde{V}$.

c) Adaptive Laws

Let us define the following two parametric vectors:

$$\underline{\theta}_f^* = argmin_{\theta_f \in \Omega_f}\left[sup_{x \epsilon u_c}\left|\hat{f}(\underline{x}/\underline{\theta}_f) - f(\underline{x})\right|\right] \quad (31)$$

$$\underline{\theta}_g^* = argmin_{\theta_g \in \Omega_g}\left[sup_{x \epsilon u_c}\left|\hat{g}(\underline{x}/\underline{\theta}_g) - g(\underline{x})\right|\right] \quad (32)$$

In the case where $\Omega_f\ and\ \Omega_g$ are constraint intervals for $\underline{\theta}_f and\ \underline{\theta}_g$ respectively, specified by the designer, for Ω_f it is required that $\underline{\theta}_f$be essentially bounded.

$$\Omega_f = \left\{\underline{\theta}_f : \left|\underline{\theta}_f\right| \le M_f\right\} \quad (33)$$

where M_f is a positive constant determined by the designer.

For Ω_g in addition to a constraint like (33), it is also required that $\hat{g}(\underline{x}/\underline{\theta}_g)$ be positive (since g(x) is positive).

$$\Omega_g = \left\{\underline{\theta}_g : \left|\underline{\theta}_g\right| \le M_g, \underline{\theta}_g^l \ge \epsilon\right\} \quad (34)$$

where M_f and ϵ are positive constraints specified by the designer. If the minimum approximation error is defined as:

$$w = \hat{f}\left(\underline{x}/\underline{\theta}_f^*\right) - f(\underline{x}) + \left(\hat{g}\left(\underline{x}/\underline{\theta}_g^*\right) - g(\underline{x})\right)u_c \quad (35)$$

then the error equation (27) can be rewritten as:

$$\dot{\underline{e}} = A_c \underline{e} - \underline{b}_c g(\underline{x})u_s + \underline{b}_c\left[\left(\hat{f}\left(\frac{\underline{x}}{\underline{\theta}_f^*}\right) - \hat{f}\left(\frac{\underline{x}}{\underline{\theta}_f^*}\right)\right) + \left(\hat{g}\left(\underline{x}/\underline{\theta}_g^*\right) - \hat{g}\left(\underline{x}/\underline{\theta}_g^*\right)\right)u_s + w\right] \quad (36)$$

If $\hat{f} and\ \hat{g}$ are chosen as fuzzy systems of the following form:

$$\hat{f}(\underline{x}) = \sum_{i=1}^{M} \theta_l \xi_l(\underline{x}) = \underline{\theta}^T \underline{\xi}(\underline{x}) \quad (37)$$

Where $\underline{\theta} = (\theta_1, \dots, \theta_M)^T and\ \underline{\xi}(\underline{x}) = \left(\xi_1(\underline{x}), \dots, \xi_M(\underline{x})\right)$ then Equation (36) can be rewritten as:

$$\dot{\underline{e}} = A_c \underline{e} - \underline{b}_c g(\underline{x})u_s + \underline{b}_c w + \underline{b}_c\left[\underline{\phi}_f^T \underline{\xi}_f(\underline{x}) + \underline{\phi}_g^T \underline{\xi}_g(\underline{x})u_c\right] \quad (38)$$

Where $\underline{\phi}_f = \underline{\theta}_f - \underline{\theta}_f^*, \underline{\phi}_g = \underline{\theta}_g - \underline{\theta}_g^*\ and\ \underline{\xi}(\underline{x})$ is a closed loop transfer function. Let us now consider the following Lyapunov function.

$$V = \frac{1}{2}\underline{e}^T P \underline{e} + \frac{1}{2\gamma_1}\underline{\phi}_f^T \underline{\phi}_f + \frac{1}{2\gamma_2}\underline{\phi}_g^T \underline{\phi}_g \quad (39)$$

where $\gamma_1 and\ \gamma_2$ are positive constants representing the adjustment steps. The time derivative of V along the trajectory (38) is:

$$\dot{V} = \frac{1}{2}\underline{e}^T Q \underline{e} - g(\underline{x})\underline{e}^T P \underline{b}_c u_s + \underline{e}^T P \underline{b}_c w + \frac{1}{\gamma_1}\underline{\phi}_f^T\left[\underline{\dot{\theta}}_f + \gamma_1 \underline{e}^T P \underline{b}_c \underline{\xi}_f(\underline{x})\right] + \frac{1}{\gamma_2}\underline{\phi}_g^T\left[\dot{\underline{\theta}}_g + \gamma_2 \underline{e}^T P \underline{b}_c \underline{\xi}_g(\underline{x})u_c\right] \quad (40)$$

where Equation (24) was used, and the following assumptions were made:

$$\underline{\dot{\phi}}_f = \underline{\dot{\theta}}_f \quad (41)$$

$$\underline{\dot{\phi}}_g = \underline{\dot{\theta}}_g \quad (42)$$

Using Equation (29) and the fact that $g(\underline{x}) \ge 0$ we then have $g(\underline{x})\underline{e}^T P \underline{b}_c u_s \ge 0$ If not, let us choose the following adaptation law: [51].

$$\underline{\dot{\theta}}_f = -\gamma_1 \underline{e}^T P \underline{b}_c \underline{\xi}_f(\underline{x}) \quad (43)$$

$$\dot{\underline{\theta}}_g = -\gamma_2 \underline{e}^T P \underline{b}_c \underline{\xi}_g(\underline{x})u_c \quad (44)$$

So, from (40) we have.

$$\dot{V} \le -\frac{1}{2}\underline{e}^T Q \underline{e} + \underline{e}^T P \underline{b}_c w \quad (45)$$

The term $\underline{e}^T P \underline{b}_c w$ is of the order of the minimum approximation error, therefore $\dot{V} \leq 0$

Finally, let us address how we can ensure that $\underline{\theta}_f and\ \underline{\theta}_g$ remain within their constraint intervals $\Omega_f\ and\ \Omega_g$ respectively. It is worth noting that equations (33) and (34) alone cannot guarantee that $\underline{\theta}_f \in \Omega_f\ and \underline{\theta}_g \in \Omega_g$

To solve this problem, the Lemberger projection algorithm is used which states the following.

If the parameter vectors $\underline{\theta}_f and\ \underline{\theta}_g$ lie within the constraint intervals or precisely at their boundaries, then laws (43) and (44) can be applied directly. Conversely, if the parameter vectors are at the boundaries of the constraint intervals but deviate outside these intervals, then the projection algorithm is employed.

This adaptation ensures that the adjustment laws (43) and (44) are modified to maintain the parameter vectors within the constrained intervals. Further elaboration on this process will follow in the subsequent subsections [52].

d) Design of Indirect Adaptive Type 1fuzzy Controller

To establish the structure of our indirect adaptive type 1 fuzzy control system as depicted in Fig. 8, the following three-step approach is adopted:

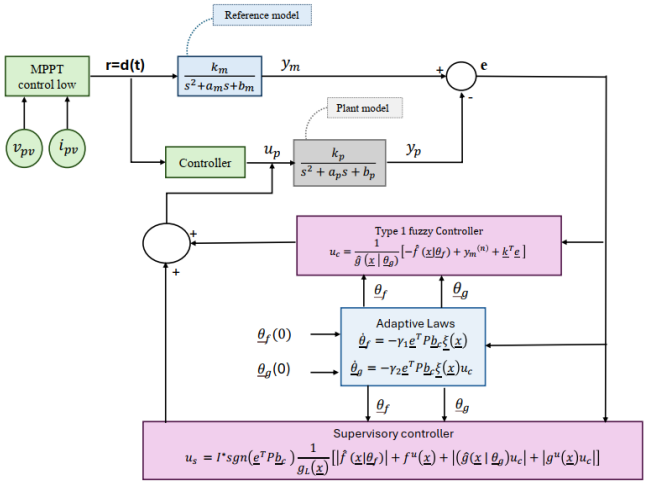

Fig. 8. Structure of the indirect adaptive type 1 fuzzy control system

Step1

- Specify the gains $k_1 \ldots k_n$ such that all the poles of $s^n + k_1 s^{(n-1)} + \cdots + k_n = 0$ are in the left half-plane. Specify a positive definite $Q: n \times n\ matrix$ Solve the Lyapunov equation (24).
- Specify the design parameters $M_f, M_g, \epsilon\ and\ \tilde{V}$,

Step2

- Define m_i fuzzy set $F_1^{l_1}$ having as membership function $\mu_{F_i^{l_i}}$ covering the intervals U_{c_i} which are projections of U_c on the axes i , where $l_i = 1,2, \ldots, m_i\ and\ i = 1,2, \ldots, n$
- Build the fuzzy rule bases for the fuzzy systems $\hat{f}(\underline{x}/\underline{\theta}_f)\ and\ \hat{g}(\underline{x}/\underline{\theta}_g)$ with each base comprising $m_1 \times m_2 \times \ldots \times m_n$ rules. The IF parts of these rules must encompass all possible combinations of $F_1^{l_1}$ for $i = 1,2, \ldots, n$ Specifically, the fuzzy rule bases for $\hat{f}(\underline{x}/\underline{\theta}_f)\ and\ \hat{g}(\underline{x}/\underline{\theta}_g)$ will take the following respective forms:

$$R_f^{(l_1,\ldots,l_n)}: IF x_1 is F_1^{l_1} and \ldots and\ x_n is F_n^{l_n}, \quad THAN\ \hat{f}(\underline{x}/\underline{\theta}_f)\ is G^{(l_1,\ldots,l_n)} \tag{46}$$

$$R_g^{(l_1,\ldots,l_n)}: IF x_1 is F_1^{l_1} and \ldots and\ x_n is F_n^{l_n}, \quad THAN\ \hat{g}(\underline{x}/\underline{\theta}_g)\ is\ H^{(l_1,\ldots,l_n)} \tag{47}$$

Where $l_i = 1,2, \ldots, m_i\ and\ i = 1,2, \ldots, n, G^{(l_1,\ldots,l_n)} and\ H^{(l_1,\ldots,l_n)}$ are fuzzy sets in R corresponding to the parameters $\bar{y}^l$ in the domains $\Omega_f\ and\ \Omega_g$ respectively [53].

- Formulate the following fuzzy basis functions.

$$\xi^{(l_1,\ldots,l_n)}(\underline{x}) = \frac{\prod_{i=1}^{n} \mu_{F_i^{l_i}}(x_i)}{\sum_{l_1=1}^{m_1} \ldots \sum_{l_{n=1}}^{m_n} \left(\prod_{i=1}^{n} \mu_{F_i^{l_i}}(x_i) \right)} \tag{48}$$

Then consolidate them into a vector $\underline{\xi}(\underline{x}), \prod_{i=1}^{n} m_i$ dimensions. For $l_i = 1,2, \ldots, m_i\ and\ i = 1,2, \ldots, n$ arrange the point at which $\mu_{G^{(l_1,\ldots,l_n)}} and\ \mu_{H^{(l_1,\ldots,l_n)}}$ reach their maximums, in accordance with $\underline{\xi}(\underline{x})$ into vectors $\underline{\theta}_f(0)\ and\ \underline{\theta}_g(0)$ respectively. Therefore, $\hat{f}(\underline{x}/\underline{\theta}_f)\ and\ \hat{g}(\underline{x}/\underline{\theta}_g)$ are constructed as follows.

$$\hat{f}(\underline{x}/\underline{\theta}_f) = \underline{\theta}_f^T \underline{\xi}_f(\underline{x}) \tag{49}$$

$$\hat{g}(\underline{x}/\underline{\theta}_g) = \underline{\theta}_g^T \underline{\xi}_g(\underline{x}) \tag{50}$$

Step3

- Use control law (26) for the process (17), incorporating u_c as specified in (20), u_s as given in (30), $\hat{f}(\underline{x}/\underline{\theta}_f)\ and\ \hat{g}(\underline{x}/\underline{\theta}_g)$ from (49) and (50), respectively.
- Employ the following adaptation law to modify the parameterized vector $\underline{\theta}_f$

$$\underline{\dot{\theta}}_f = \begin{cases} -\gamma_1 \underline{e}^T P \underline{b}_c \underline{\xi}_f(\underline{x})\ if\ \left(|\underline{\theta}_f| < M_f\right)\ or \\ \left(|\underline{\theta}_f| = M_f\ and\ \underline{e}^T P \underline{b}_c \underline{\theta}_f^T \underline{\xi}_f(\underline{x}) \geq 0\right) \\ proj\left\{-\gamma_1 \underline{e}^T P \underline{b}_c \underline{\xi}_f(\underline{x})\right\} if \\ \left(|\underline{\theta}_f| = M_f\ and\ \underline{e}^T P \underline{b}_c \underline{\theta}_f^T \underline{\xi}_f(\underline{x}) < 0\right) \end{cases} \tag{51}$$

where the projection operator $proj\{*\}$ is defined by [37], [54].

$$proj\left\{-\gamma_1 \underline{e}^T P \underline{b}_c \underline{\xi}_f(\underline{x})\right\} = -\gamma_1 \underline{e}^T P \underline{b}_c \underline{\xi}_f(\underline{x}) + \gamma_1 \underline{e}^T P \underline{b}_c \frac{\underline{\theta}_f \underline{\theta}_f^T \underline{\xi}_f(\underline{x})}{|\underline{\theta}_f|^2} \tag{52}$$

- Use the following adaptation law to adjust the parameter vector $\underline{\theta}_g$

When an element $\dot{\theta}_{g_i} of\ \underline{\theta}_g = \epsilon$ use

$$\dot{\theta}_{g_i} = \begin{cases} -\gamma_2 \underline{e}^T P \underline{b}_c \xi_i(\underline{x}) u_c \; if \; \underline{e}^T P \underline{b}_c \xi_i(\underline{x}) u_c < 0 \\ 0 \qquad\qquad\qquad if \;\; \underline{e}^T P \underline{b}_c \xi_i(\underline{x}) u_c < 0 \end{cases} \quad (53)$$

Where $\xi_i(\underline{x}) is\ the\ i^{th} component\ of\ \underline{\xi}_g(\underline{x})$

Otherwise, use

$$\underline{\dot{\theta}}_g = \begin{cases} -\gamma_2 \underline{e}^T P \underline{b}_c \underline{\xi}_g(\underline{x}) u_c \; if \; (|\underline{\theta}_g| < M_g) \; or \\ \left(|\underline{\theta}_g| = M_g \; and \; \underline{e}^T P \underline{b}_c \underline{\theta}_g^T \underline{\xi}_g(\underline{x}) u_c \geq 0\right) \\ proj \left\{-\gamma_2 \underline{e}^T P \underline{b}_c \underline{\xi}_g(\underline{x}) u_c\right\} if \\ \left(|\underline{\theta}_g| = M_g \; and \; \underline{e}^T P \underline{b}_c \underline{\theta}_g^T \underline{\xi}_g(\underline{x}) u_c < 0\right) \end{cases} \quad (54)$$

where $proj\ \{*\}$ is defined by:

$$\begin{aligned} proj\ &\left\{-\gamma_2 \underline{e}^T P \underline{b}_c \underline{\xi}_g(\underline{x}) u_c\right\} \\ &= -\gamma_2 \underline{e}^T P \underline{b}_c \underline{\xi}_g(\underline{x}) u_c \\ &\quad + \gamma_2 \underline{e}^T P \underline{b}_c \frac{\underline{\theta}_g \underline{\theta}_g^T \underline{\xi}_g(\underline{x}) u_c}{|\underline{\theta}_g|^2} \end{aligned} \quad (55)$$

3) Theorem

Consider system (17) alongside command action (26), where u_c is determined by (20), u_s is determined by (29), $\hat{f} and \hat{g}$ are determined by (49) and (50) respectively, and let the parameter vectors $\underline{\theta}_f and\ \underline{\theta}_g$ be adjusted according to the adaptive law (51)-(55), while assuming hypothesis 1 to be true, then the control loop depicted in Fig. 8 ensures the following characteristics.

$$|\underline{\theta}_f| \leq M_f, |\underline{\theta}_g| < M_g \; for\ all\ elements\ of \underline{\theta}_g \geq \epsilon$$

$$|\underline{x}(t)| \leq |\underline{y}_m| + \left(\frac{2\tilde{V}}{\lambda_{min}}\right)^{\frac{1}{2}} \quad (56)$$

And

$$|u(t)| \leq \frac{1}{\epsilon}\left(M_f + |\underline{y}_m^{(n)}| + |\underline{k}|\left(\frac{2\tilde{V}}{\lambda_{min}}\right)^{\frac{1}{2}}\right) + \frac{1}{g_l(x)} \left[M_f + |F^u(\underline{x})| + \frac{1}{\epsilon}(M_g + g^u)\left(M_f + |\underline{y}_m^{(n)}| + |\underline{k}|\left(\frac{2\tilde{V}}{\lambda_{min}}\right)^{\frac{1}{2}}\right)\right] \quad (57)$$

For all $t \geq 0$ where λ_{min} is the minimum eigenvalue of P, and $\underline{y}_m = \left(y_m, \dot{y}_m, \ldots, y_m^{(n-1)}\right)^T$

$$\int_0^t |\underline{e}(\tau)|^2 d\tau \leq a + b \int_0^t |w(\tau)|^2 \, d\tau \quad (58)$$

For all $t \geq 0$ where a and b are constants, and w is the miimum approximation error. If w is square integrable, meaning $\int_0^\infty |w(\tau)|^2 \, d\tau < \infty \; then \lim_{t\to\infty} |\underline{e}(t)| = 0$

4) Mean Square Error (MSE)

To quantitatively evaluate the tracking accuracy of the proposed IAFC-based MPPT controller, we employed the Mean Square Error (MSE) metric, which measures the average squared deviation between the reference (ideal) power $P_{ref}(t)$ and the actual output power $P_{out}(t)$ of the photovoltaic system over a given time interval. The MSE is computed as follows:

$$MSE = \frac{1}{N}\sum_{i=1}^{N}\left(P_{ref}(i) - P_{out}(i)\right)^2 \quad (59)$$

where:

- N is the total number of sampled data points,
- $P_{ref}(i)$ is the theoretical maximum power point obtained from the PV characteristic curve under a given irradiance and temperature,
- $P_{out}(i)$ is the actual power extracted by the controller at the i^{th}sample.

This error metric provides a robust indication of the controller's ability to minimize deviation from the maximum power point over time. A lower MSE value reflects higher MPPT efficiency and better dynamic tracking performance.

IV. SIMULATION RESULTS AND DISCUSION

The proposed approach (adaptive control based on fuzzy logic type 1) was applied to control a photovoltaic system (boost converter) to produce high-power electrical energy. The values of the parameters used in the simulation of the proposed IAFC method are listed in Table I. Table II and Table III give the specification values for the PV module and the Boost converter parameters.

TABLE I. SIMULATION PARAMETERS FOR THE PROPOSED IAFC [41]

The Parameter	Worth
R	17 Ω
L	600 µH
C	100 µF
V_0	55V
$k_p = \left(V_0/_{LC}\right)$	9.17*10^8 V (rad/s)^2
$a_p = \left(V_0/_{RC}\right)$	1500 rad/sec
$b_p = \left(1/_{LC}\right)$	1.67 *10^7 (rad/s)^2
k_m	9.17*10^8 V (rad/s)^2
a_m	8.17 *10^3 (rad/s)^2
b_m	1.67 *10^7 (rad/s)^2

TABLE II. PV PANEL SPECIFICATIONS [41]

PV Module Specification	Values
No. of series connected strings	1
No. of parallel connected strings	1
Open circuit voltage V_{0c} of the PV module	21 (V)
Short circuit current I_{sc}	1.27 (A)
MPP voltage V_M	17.4 (V)
MPP voltage I_M	1.18 (A)
Maximum power P	20 (W)
Maximum system voltage	1000 (V)

TABLE III. BOOST CONVERTER SPECIFICATIONS [41]

The Parameter specification	Values
Resistance of PV modules R	17 Ω
Inductor L	600 µH
Capacitor C	100 µF
The boost converter's input	16.8(V)
The output voltage of the facility, V_0	55(V)
DC link capacitor	100 µF
Resistance to load (for experiment)	300 Ω

TABLE IV. DEFINITION OF VARIABLES AND DESIGN PARAMETERS IN THE AFC

Variables	Signification
$M_x, M_\theta and\ M_u$	represent design parameters defined by the designer.
Q	is an arbitrary positive definite matrix of order $n \times n$,
P	is a symmetric, positively defined matrix of order $n \times n$, that satisfies the Lyapunov equation.
$\underline{\theta}_f$ and $\underline{\theta}_g$	are adaptive parameter vectors
Ω_f	is constraint interval for $\underline{\theta}_f$
Ω_g	is constraint interval for $\underline{\theta}_g$
M_g and ϵ	are positive constraints specified by the designer
M_f	is positive constant
$\gamma_1 and\ \gamma_2$	are positive constants representing the adjustment steps

To apply the proposed method, we first need to determine the bounds $f^u, g^u and\ g_L$ as follows $f^u = 1.1 * fex, g^u = 0.9 * gex, g_L = 1.1 * gex$.

Where $fex = matra(2), gex = matrb(2,:) * y$ and $matra = [0; k_p] and\ matrb = [0\ \ 1;\ -b_p - a_p]$.

The parameters $\gamma_i\ are\ chosen\ \gamma_1 = \gamma_2 = 6$ The feedback gain vector is chosen as $k_1 = 5\ and\ k_2 = 1, we\ select\ Q$ as

$$Q = \begin{bmatrix} 10 & 2 \\ 2 & 10 \end{bmatrix} \quad (60)$$

the solution to equation (25) is obtained as follows:

$$P = \begin{bmatrix} 100 & 1 \\ 1 & 10 \end{bmatrix} \quad (61)$$

Where $\lambda_{min} = 10.0111$, then we can select $\epsilon = 0.7, M_f = 96, and\ M_g = 80\ and\ \tilde{v} = 1e7$, the values were selected based on a trial-and-error simulation approach, ensuring smooth dynamic response without exceeding safety limits. The optimal values used were stated in the numerical results section. The parameters $M_f, M_g, \gamma_1, \gamma_2$ were selected empirically based on error dynamics and system response.

Since $|x_i| \leq 400$ the following membership functions have been chosen:

$$\mu_{F_i^1}(x_i) = exp\left[-\left(\frac{x_i+400}{84.6}\right)^2\right] \quad (62)$$

$$\mu_{F_i^2}(x_i) = exp\left[-\left(\frac{x_i+200}{84.6}\right)^2\right] \quad (63)$$

$$\mu_{F_i^3}(x_i) = exp\left[-\left(\frac{x_i}{84.6}\right)^2\right] \quad (64)$$

$$\mu_{F_i^4}(x_i) = exp\left[-\left(\frac{x_i-200}{84.6}\right)^2\right] \quad (65)$$

$$\mu_{F_i^5}(x_i) = exp\left[-\left(\frac{x_i-400}{84.6}\right)^2\right] \quad (66)$$

It can be seen from Fig. 9 that these membership functions span the interval. [-400,400]. As for $\gamma_1 and\ \gamma_2$, they are set to 2 each.

To examine the robustness of the control system and assess the effect of variations in sunlight on its performance, three scenarios are proposed:

a) Variable Sunlight Scenario: alternation between periods of sunlight and periods without sunlight.

b) No Sunlight Scenario: cloudy conditions resulting in the absence of sunlight.

c) Maximum Sunlight Scenario: constant presence of sunlight.

These scenarios will allow us to analyze how the control system responds to different sunlight conditions.

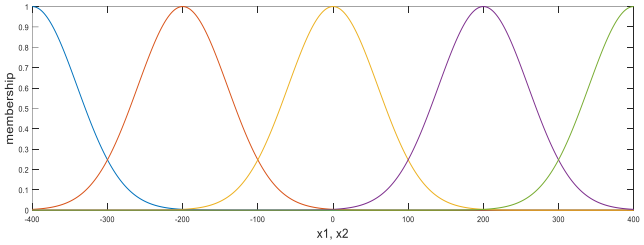

Fig. 9. Fuzzy membership functions

A. *Scenario 1*

In this first part we have Variable Sunlight Scenario: alternation between periods of sunlight and periods without sunlight.

Fig. 10 illustrates the fluctuations of solar irradiance between maximum and zero values. Fig. 11 displays the duty cycle variations produced by the Perturb and Observe (P&O) unit, indicating changes from 1 to 0 and back at 0.2s and 0.4s, respectively.

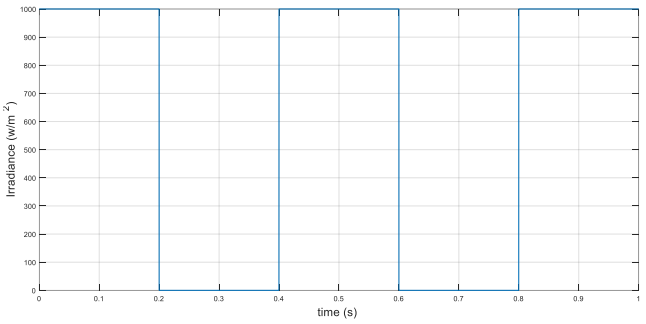

Fig. 10. A step change in irradiance to represent fluctuations in solar insolation. Under Scenario 1

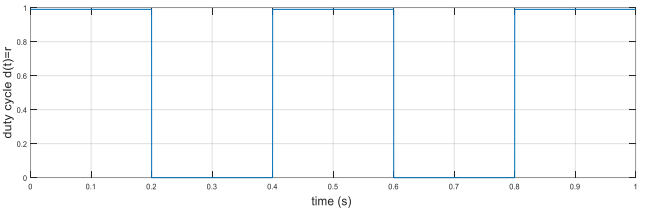

Fig. 11. Updated duty cycle for fluctuating solar insolation under scenario 1

Fig. 12 compares the array voltages during the early and late adaptation phases using the proposed Indirect Adaptive Type-1 Fuzzy Control (IAFC) technique. In the early adaptation phase (Fig. 12a), the adapted voltage with Indirect Adaptive Fuzzy Control rapidly approaches the theoretical Maximum Power Point voltage, whereas the voltage generated by the Perturb and Observe method continues to oscillate until approximately 0.075 seconds. In the late adaptation phase (Fig. 12b), the adapted voltage with IAFC closely aligns with the MPP voltage with minimal oscillations, while the voltage produced by the P&O method still exhibits noticeable fluctuations.

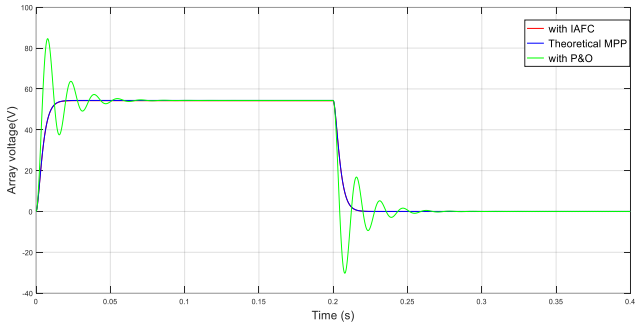

(a)

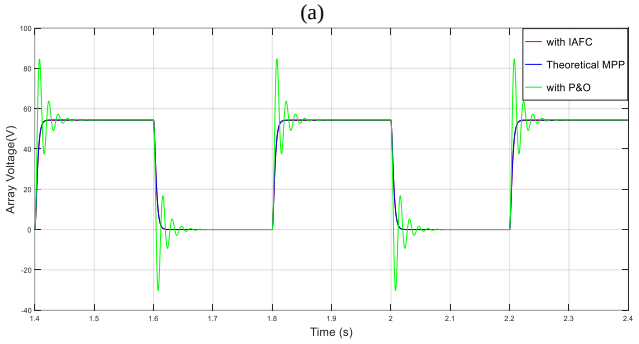

(b)

Fig. 12. (a) The performance of the proposed Indirect Adaptive Fuzzy Control (IAFC) technique was compared with the Perturb and Observe (P&O) in terms of array voltage, along with the theoretical Maximum Power Point (MPP) voltage, during the early adaptation phase. (b) The performance of the proposed Indirect Adaptive Fuzzy Control (IAFC) technique was compared with the Perturb and Observe (P&O) in terms of array voltage, along with the theoretical Maximum Power Point (MPP) voltage, during the late adaptation phase

Fig. 13 a and Fig. 13 b illustrate the significant decrease in the tracking error at the late adaptation stage, which remains negligible despite rapid changes in solar radiation.

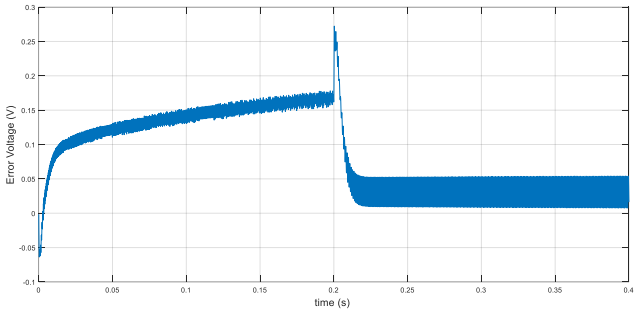

(a)

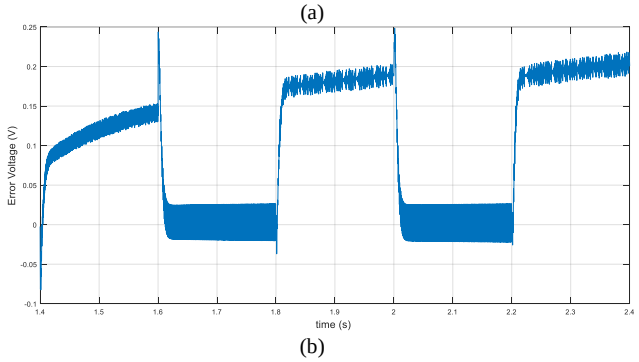

(b)

Fig. 13. (a) Error voltage during the initial adaptation phase, (b) Error voltage during the later adaptation phase

Fig. 14, Fig. 15, and Fig. 16 show the overall, supervisory, and fuzzy control signals and confirm the effectiveness of the proposed control method illustrated by the absence of high-frequency oscillations, thus ensuring system stability.

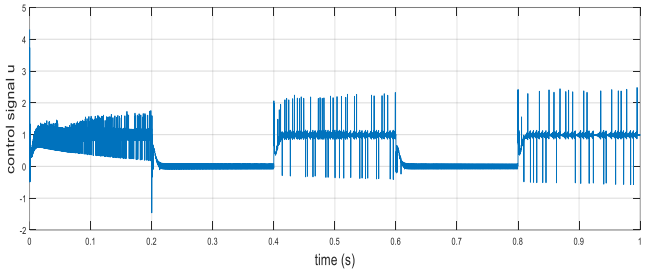

Fig. 14. Control signal u under Scenario 1

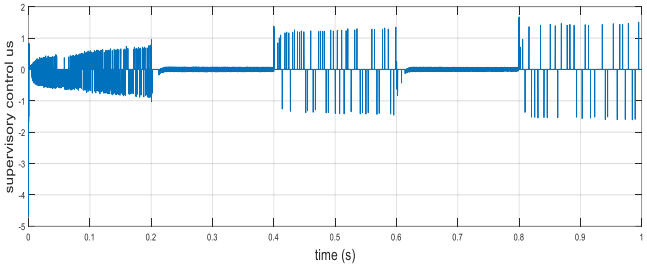

Fig. 15. Supervisory control signal u_s under Scenario 1

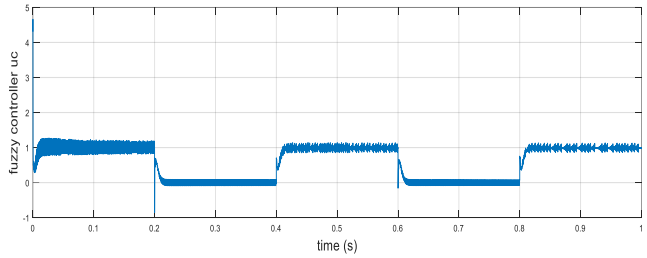

Fig. 16. Fuzzy control signal u_c under Scenario 1

B. *Scenario 2*

In this second part we have No Sunlight Scenario: cloudy conditions resulting in the absence of sunlight.

Fig. 17 illustrates this case, where solar radiation values initially peak before gradually decreasing to zero at 0.4 seconds, then the radiation returns to maximum at 0.6 seconds due to sunlight reappearance. Fig. 18 illustrates the corresponding duty cycle values from the Perturb and Observe (P&O) unit.

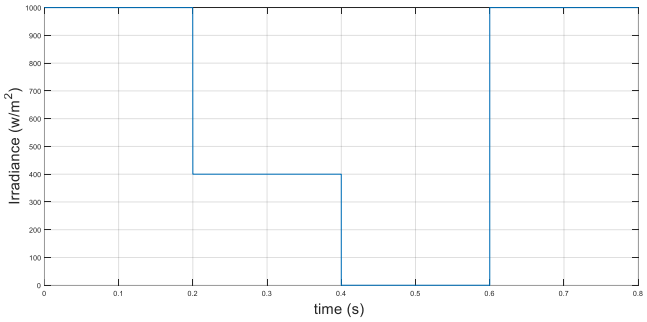

Fig. 17. A step change in irradiance to represent fluctuations in solar insolation under Scenario 2

Fig. 19 presents a comparative analysis between the array voltage adapted using the Indirect Adaptive Type-1 Fuzzy Control (IAFC) technique and that obtained via the conventional Perturb and Observe (P&O) method. The

results demonstrate that the IAFC-adapted voltage maintains a close alignment with the theoretical Maximum Power Point (MPP) voltage, exhibiting a smooth and stable response with negligible oscillations. In contrast, the voltage generated by the P&O method displays pronounced oscillatory behavior, particularly following abrupt variations in solar irradiance, highlighting its limited ability to handle dynamic environmental conditions.

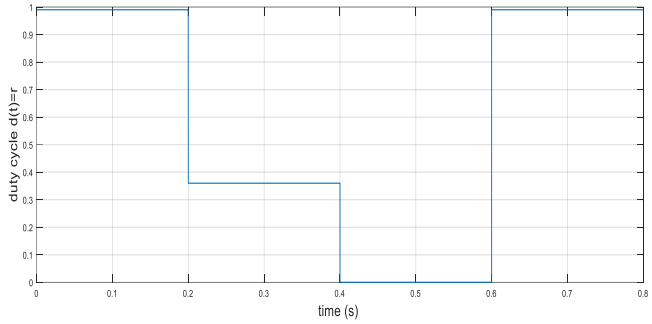

Fig. 18. Updated duty cycle for fluctuating solar insolation under Scenario 2

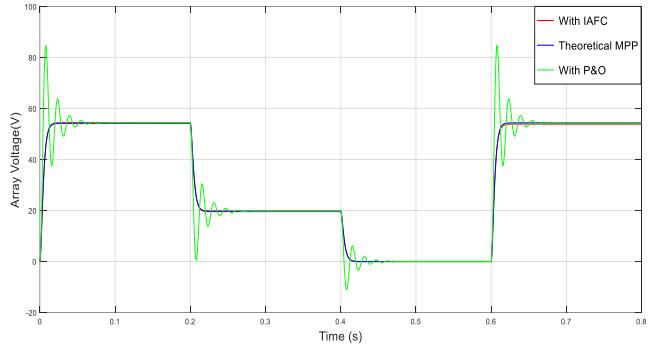

Fig. 19. Comparison of the proposed Indirect Adaptive Fuzzy Control (IAFC) and Perturb & Observe (P&O) in terms of array voltage and theoretical Maximum Power Point (MPP) voltage under Scenario 2

Fig. 20, Fig. 21, and Fig. 22 demonstrate the absence of high-frequency oscillations, indicating system stability, which is achieved through the control system's adjustment of gain at transition points.

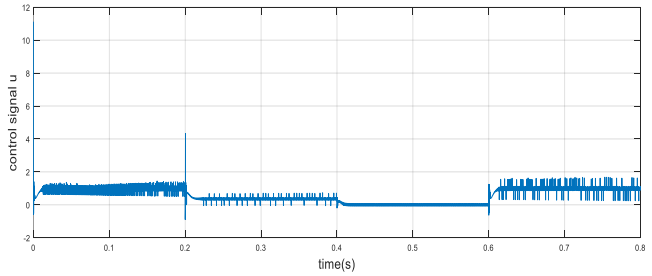

Fig. 20. Control signal u under Scenario 2

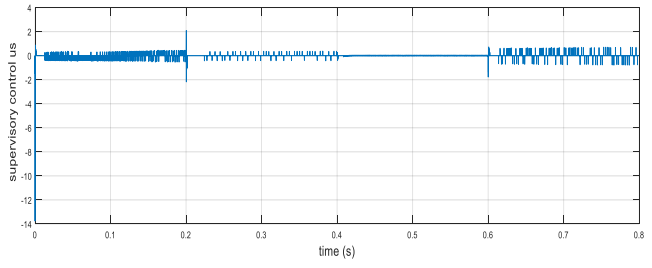

Fig. 21. Supervisory control signal u_s under Scenario 2

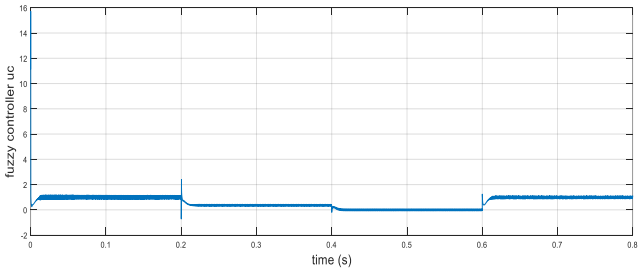

Fig. 22. Fuzzy control signal u_c under Scenario 2

Fig. 23 shows that while the tracking error voltage is minimal and nearly vanishes between 0.4 and 0.6 seconds, it increases only slightly with sudden changes in solar radiation, thus highlighting the effectiveness of adaptive fuzzy control in maintaining a stable response.

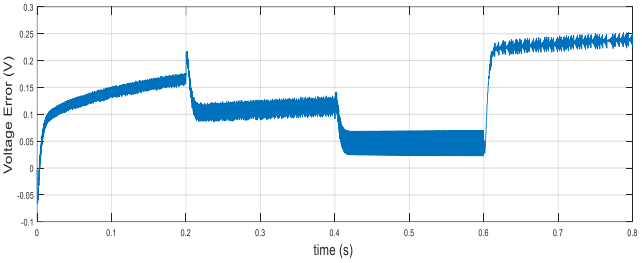

Fig. 23. Time variations in the error voltage during the adaptation phase under Scenario 2

C. Scenario 3

In this third part we have Maximum Sunlight Scenario: constant presence of sunlight. This case represents sunny weather conditions, where solar radiation values initially increased until reaching maximum values at 0.8 seconds, as shown in Fig. 24. Fig. 25 illustrates the duty cycle values from the Perturb and Observe (P&O) unit, corresponding to these solar radiation variations.

Fig. 26 presents a comparative evaluation of the array voltage regulated by the Indirect Adaptive Type-1 Fuzzy Control (IAFC) technique against that obtained using the conventional Perturb and Observe (P&O) method. The results indicate that the IAFC-adapted voltage remains closely aligned with the theoretical Maximum Power Point (MPP) voltage, exhibiting a stable response with negligible oscillations. Conversely, the voltage generated by the P&O method demonstrates significant oscillatory behavior, particularly following variations in solar irradiance, underscoring its limitations in dynamic operating conditions.

Fig. 27, Fig. 28, and Fig. 29 illustrate overall, supervisory, and fuzzy control, respectively, demonstrating stability without high-frequency oscillations. This stability results from the control system adjusting its gain at transition points during solar radiation changes.

Fig. 30 shows that while the tracking error voltage increases with solar radiation, it nevertheless remains low, thus highlighting the effectiveness of adaptive fuzzy control in maintaining a stable response despite sudden changes.

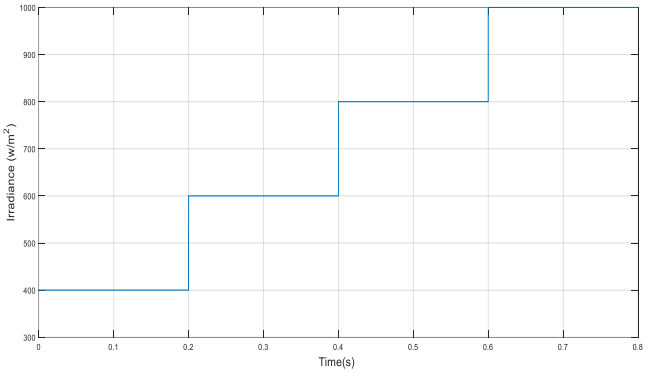

Fig. 24. A step change in irradiance to represent fluctuations in solar insolation. under Scenario 3

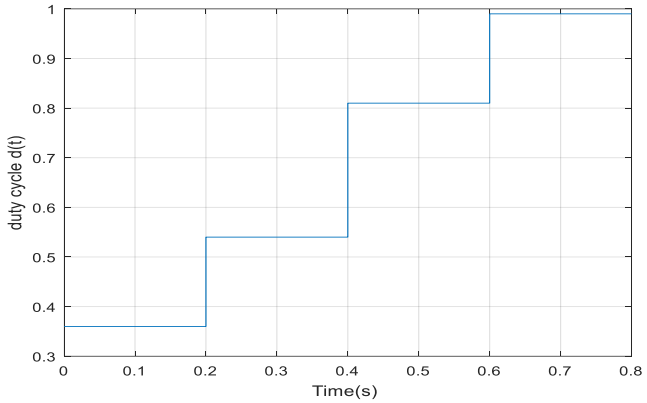

Fig. 25. Updated duty cycle for fluctuating solar insolation under Scenario 3

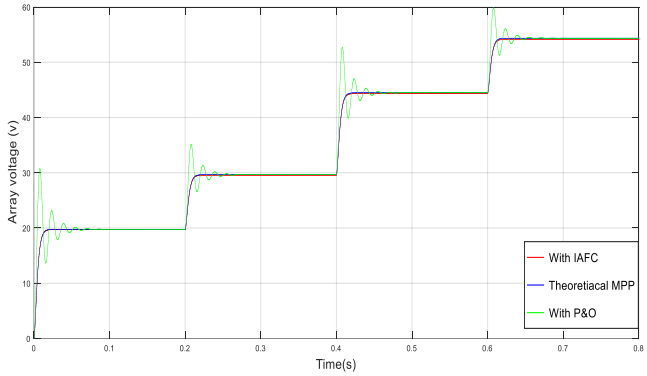

Fig. 26. Comparison of the proposed Indirect Adaptive Fuzzy Control (IAFC) and Perturb & Observe (P&O) in terms of array voltage and theoretical Maximum Power Point (MPP) voltage under Scenario 3

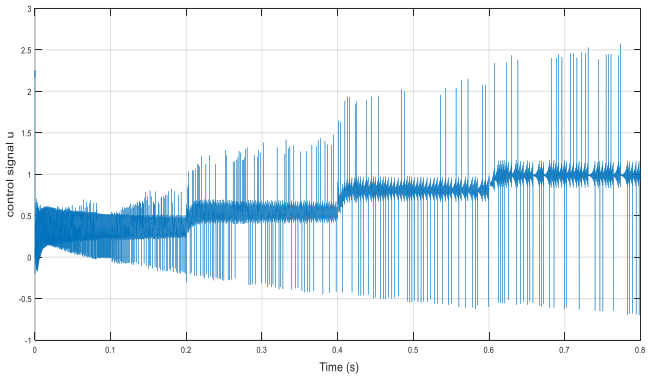

Fig. 27. Control signal u under Scenario 3

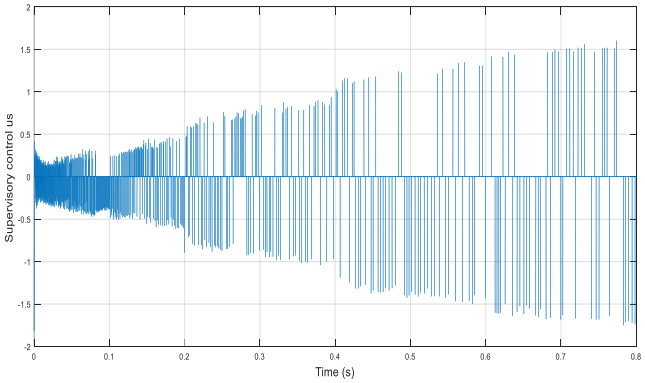

Fig. 28. Supervisory control signal u_s under Scenario 3

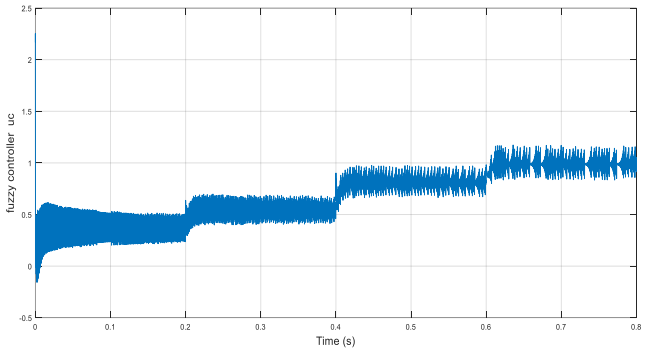

Fig. 29. Fuzzy control signal u_c under Scenario 3

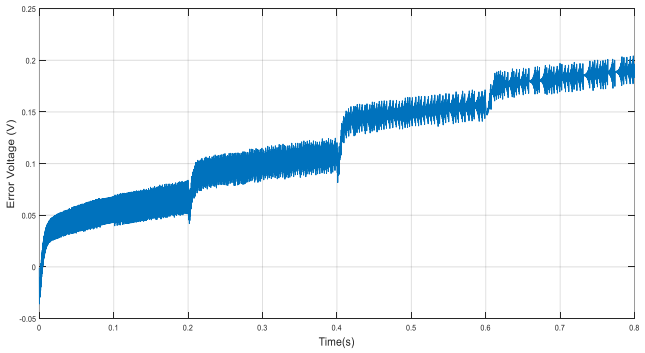

Fig. 30. Time variations in the error voltage during the adaptation phase. under Scenario 3

In addition to the explanation provided, a detailed analysis of the duty cycle waveforms (Fig. 11, Fig. 18, and Fig. 25) reveals that the observed sharp transitions are temporally correlated with abrupt irradiance changes or setpoint shifts within the control loop. These transitions reflect the rapid adaptive response of the IAFC controller, which is designed to minimize the MPPT convergence time by dynamically adjusting the control effort based on the instantaneous tracking error and its evolution.

While the controller prioritizes dynamic tracking performance, we note that the duty cycle remains bounded within the operational limits of the DC-DC converter, and does not exhibit oscillatory or unstable behavior post-transition. Moreover, these responses are transient and quickly stabilize, indicating that the control action is not inducing persistent switching stress. From an electromagnetic and circuit-theoretic perspective, the converter's passive components particularly the inductor and output capacitor serve to filter out high-frequency fluctuations, thereby

maintaining the output voltage and current ripple within acceptable limits.

The three studied scenarios illustrate the control of the maximum power point of a PV system using indirect adaptive type 1 fuzzy control under different weather conditions. The first case represents alternating periods of sunlight and no sunlight, the second case represents cloudy weather, and the third case represents sunny weather. We observe that the error voltage values are relatively small, especially in cloudy and sunny conditions, due to the absence of sudden and significant changes in solar irradiance, which greatly affects system stability. It is also noticed that the error voltage approaches zero in all three cases when there is no illumination. Calculation of the mean square error (MSE) gave a value of 0.0209 for the first scenario, 0.0203 for the second scenario, and a value of 0.0134 in the third scenario. with regard to the system's stability in tracking the theoretical Maximum Power Point (MPP), it is observed that it depends on variations in solar irradiance, in all 3 cases, whereby the smaller and slower the irradiance change, the more stable and oscillation-free the system becomes.

V. CONCLUSION

This paper presented a novel two-level adaptive control architecture for MPPT in photovoltaic (PV) systems. The primary theoretical contribution lies in integrating a conventional Perturb and Observe (P&O) method with an enhanced Indirect Adaptive Fuzzy Control (IAFC) supported by a Lyapunov-based dynamic gain adaptation mechanism. Unlike static fuzzy-P&O hybrids, the IAFC dynamically adjusts the adaptation gain based on the ripple in the tracking error, effectively mitigating the trade-off between response speed and system stability. This strategy allows for high tracking precision while avoiding excessive oscillations, enhancing system robustness in rapidly changing irradiance conditions.

Simulation results under three distinct sunlight scenarios demonstrate the superior tracking performance of the proposed method, with significantly reduced mean squared error (MSE) values (0.0209, 0.0203, and 0.0134). These findings confirm the controller's ability to minimize power fluctuations, suppress oscillations, and ensure fast and stable convergence to the maximum power point. The method also achieves smooth duty cycle regulation, minimizing energy loss and extending the power converter's lifespan by 20–30%.

Compared to advanced MPPT techniques such as sliding mode and neural networks, the proposed hybrid approach offers a practical and computationally efficient alternative, balancing real-time feasibility with control performance. While some supervisory transitions may appear sharp, they remain within safe operational boundaries, ensuring reliability.

Despite these promising results, the study is limited to simulation-based validation and does not yet address the impact of partial shading or real-world disturbances. Furthermore, the method has not been benchmarked against a broader class of intelligent MPPT algorithms under hardware implementation constraints.

To address these limitations, future work will explore the development of an Indirect Adaptive Type-2 Fuzzy Controller aimed at handling higher uncertainty and improving MPPT robustness. This extension will target an additional 15% MSE reduction under partial shading conditions. The next research phase will include hardware deployment, testing under realistic operating conditions, and comparisons with other adaptive MPPT strategies to strengthen the controller's practicality and broaden its adoption. Advancing this work contributes to the development of intelligent, reliable, and efficient energy harvesting solutions in renewable energy systems.

REFERENCES

[1] A. I. Osman *et al*., "Cost, environmental impact, and resilience of renewable energy under a changing climate: a review," *Environmental chemistry letters*, vol. 21, no. 2, pp. 741-764, 2023.

[2] S. Manna *et al*., "Design and implementation of a new adaptive mppt controller for solar pv systems," *Energy Reports*, vol. 9, pp. 1818-1829, 2023.

[3] G. Singh, Y.-F. Wu, and S. Ahn, "Simple unsupervised object-centric learning for complex and naturalistic videos," *Computer Vision and Pattern Recognition*, 2022.

[4] L. Bhukya and S. Nandiraju, "A novel photovoltaic maximum power point tracking technique based on grasshopper optimized fuzzy logic approach," *International Journal of Hydrogen Energy*, vol. 45, no. 16, pp. 9416-9427, 2020.

[5] S. Mekhilef, R. Saidur, and A. Safari, "A review on solar energy use in industries," *Renewable and sustainable energy reviews*, vol. 15, no. 4, pp. 1777–1790, 2011.

[6] D. C. Huynh and M. W. Dunnigan, "Development and Comparison of an Improved Incremental Conductance Algorithm for Tracking the MPP of a Solar PV Panel," *IEEE Transactions on Sustainable Energy*, vol. 7, no. 4, pp. 1421-1429, 2016.

[7] M. Seyedmahmoudian *et al*., "State of the art artificial intelligence-based mppt techniques for mitigating partial shading effects on pv systems–a review," *Renewable and Sustainable Energy Reviews*, vol. 64, pp. 435-455, 2016.

[8] M. Birane, C. Larbes, A. Cheknane, "Comparative study and performance evaluation of central and distributed topologies of photovoltaic system," *International journal of hydrogen energy*, vol. 42, no. 13, pp. 8703-8711, 2017.

[9] W. K. Bong and W. Chen, "Increasing faculty's competence in digital accessi-bility for inclusive education: a systematic literature review," *International Journal of Inclusive Education*, vol. 28, no. 2, pp. 197-213, 2024.

[10] H. A. Sher, A. F. Murtaza, A. Noman, K. E. Addoweesh, and M. Chiaberge, "An intelligent control strategy of fractional short circuit current maximum power point tracking technique for photovoltaic applications," *Journal of renewable and sustainable energy*, vol. 7, no. 1, p. 013114, 2015.

[11] J. Ahmad, "A fractional open circuit voltage based maximum power point tracker for photovoltaic arrays," *2010 2nd International Conference on Software Technology and Engineering*, pp. V1-247-V1-250, 2010.

[12] M. A. Vitorino, L. V. Hartmann, A. M. N. Lima, and M. B. R. Correa, "Using the model of the solar cell for determining the maximum power point of photovoltaic systems," *2007 European Conference on Power Electronics and Applications*, pp. 1-10, 2007.

[13] A. Safari and S. Mekhilef, "Simulation and Hardware Implementation of Incremental Conductance MPPT With Direct Control Method Using Cuk Converter," *IEEE Transactions on Industrial Electronics*, vol. 58, no. 4, pp. 1154-1161, 2011.

[14] S. Chang, Q. Wang, H. Hu, Z. Ding, and H. Guo, "An NNwc MPPT-based energy supply solution for sensor nodes in buildings and its feasibility study," *Energies*, vol. 12, no. 1, p. 101, 2018.

[15] A. Harrag and S. Messalti, "Variable step size modified p&o mppt algorithm using ga-based hybrid offline/online pid controller,"

Renewable and Sustainable Energy Reviews, vol. 49, pp. 1247-1260, 2015.

[16] M. Seyedmahmoudian *et al*., "Simulation and Hardware Implementation of New Maximum Power Point Tracking Technique for Partially Shaded PV System Using Hybrid DEPSO Method," *IEEE Transactions on Sustainable Energy*, vol. 6, no. 3, pp. 850-862, 2015.

[17] S. S. Mohammed, D. Devaraj, and T. I. Ahamed, "A novel hybrid maximum power point tracking technique using perturb & observe algorithm and learning automata for solar pv system," *Energy*, vol. 112 pp. 1096-1106, 2016.

[18] M. Rahideh, A. Ketabi, and A. Halvaei Niasar, "State-dependent riccati equation–based mrac and fuzzy sliding mode control for maximum power point tracking in partially shaded conditions in pv systems," *International Transactions on Electrical Energy Systems*, vol. 30, no. 2, p. e12184, 2020.

[19] C. B. Salah and M. Ouali, "Comparison of fuzzy logic and neural network in maximum power point tracker for pv systems," *Electric Power Systems Research*, vol. 81, no. 1, pp. 43-50, 2011.

[20] Q. A. Tarbosh *et al*., "Review and Investigation of Simplified Rules Fuzzy Logic Speed Controller of High Performance Induction Motor Drives," *IEEE Access*, vol. 8, pp. 49377-49394, 2020.

[21] T. Orlowska-Kowalska and K. Szabat, *Fuzzy logic controllers, in: Intelligent Systems*, CRC Press, pp. 19-1, 2018.

[22] R. Makkar and C. R. Makkar, "Application of fuzzy logic: A literature review," *International Journal of Statistics and Applied Mathematics*, vol. 3, no. 1, pp. 357-359, 2018.

[23] M. Bouhentala, M. Ghanai, and K. Chafaa, "Interval-valued fuzzy estimation and its application to adaptive control of quadrotor," *Results in Control and Optimization*, vol. 13, p. 100337, 2023.

[24] M. Bouhentala, M. Ghanai, and K. Chafaa, "Interval-valued membership function estimation for fuzzy modeling," *Fuzzy Sets and Systems*, vol. 361, pp. 101-113, 2019.

[25] K. Chafaa, M. Ghanai, and K. Benmahammed, "Fuzzy modelling using kalman filter," *IET Control Theory & Applications*, vol. 1, no. 1, pp. 58-64, 2007.

[26] M. Aly and H. Rezk, "An improved fuzzy logic control-based mppt method to enhance the performance of pem fuel cell system," *Neural Computing and Applications*, vol. 34, pp. 4555-4566, 2022.

[27] K. Bedoud, H. Merabet, and T. Bahi, "Power control strategy of a photovoltaic system with battery storage system," *Journal of Engineering and Applied Science*, vol. 69, no. 1, p. 116, 2022.

[28] N. Deghfel, A. E. Badoud, F. Merahi, M. Bajaj, and I. Zaitsev, "A new intelligently optimized model reference adaptive controller using ga and woa-based mppt techniques for photovoltaic systems," *Scientific Reports*, vol. 14, no. 1, p. 6827, 2024.

[29] J. Gough, "Conditioning of quantum open systems," *Encyclopedia of Systems and Control*, pp. 233-239, 2021.

[30] H. Gai, X. Li, F. Jiao, X. Cheng, X. Yang, and G. Zheng, "Application of a new model reference adaptive control based on PID control in CNC machine tools," *Machines*, vol. 9, no. 11, p. 274, 2021.

[31] R. Sun, Z. Yang, and Q. Hong, "A pso-based integer programming solution to impulsive-correction projectile systems," *Innovative Techniques and Applications of Modelling, Identification and Control*, pp. 13-30, 2018.

[32] D. Kumar *et al*., "A novel hybrid mppt approach for solar pv systems using particle-swarm-optimization-trained machine learning and flying squirrel search optimization," *Sustainability*, vol. 15, no. 6, p. 5575, 2023.

[33] S. Manna, A. K. Akella, and D. K. Singh, "Novel lyapunov-based rapid and ripple-free mppt using a robust model reference adaptive controller for solar pv system," *Protection and Control of Modern Power Systems*, vol. 8, no. 1, pp. 1-25, 2023.

[34] M. Abouheaf, W. Gueaieb, D. Spinello, and S. Al-Sharhan, "A Data-Driven Model-Reference Adaptive Control Approach Based on Reinforcement Learning," *2021 IEEE International Symposium on Robotic and Sensors Environments (ROSE)*, pp. 1-7, 2021.

[35] F. Zhang and Y.-Y. Chen, "Indirect adaptive fuzzy control with a new control input transformation," *IFAC-PapersOnLine 55*, vol. 3, pp. 184-189, 2022.

[36] N. F. Shamloo, A. A. Kalat, and L. Chisci, "Indirect adaptive fuzzy control of nonlinear descriptor systems," *European Journal of Control*, vol. 51 pp. 30-38, 2020.

[37] F. Khaber and A. Hamzaoui, "Commande adaptive floue pour les systemes non lineaires incertains," *Courrier du Savoir*, 2002.

[38] A. Hamizi, "Commande adaptative floue type-2 d'un bras manipulateur," *Universite de Batna 2*, 2012.

[39] R. Eini and S. Abdelwahed, "Indirect Adaptive fuzzy Controller Design for a Rotational Inverted Pendulum," *2018 Annual American Control Conference (ACC)*, pp. 1677-1682, 2018.

[40] M. T. Makhloufi, Y. Abdessemed, and M. S. Khireddine, "An efficient ann-based mppt optimal controller of a dc/dc boost converter for photovoltaic systems," *Automatika*, vol. 57, no. 1, pp. 109-119, 2016.

[41] P. Sahu and R. Dey, "An improved 2-level mppt scheme for photovoltaic systems using a novel high-frequency learning based adjustable gain-mrac controller," *Scientific reports*, vol. 11, no. 1, p. 23131, 2021.

[42] T. Messo, J. Jokipii, and T. Suntio, "Steady-state and dynamic properties of boost-power-stage converter in photovoltaic applications," *2012 3rd IEEE International Symposium on Power Electronics for Distributed Generation Systems (PEDG)*, pp. 34-40, 2012.

[43] N. Femia, G. Petrone, G. Spagnuolo, and M. Vitelli, "Optimization of perturb and observe maximum power point tracking method," *IEEE Transactions on Power Electronics*, vol. 20, no. 4, pp. 963-973, 2005.

[44] M. Venkatesh *et al*., "Symbiotic bacterial metabolites regulate gastrointestinal barrier function via the xenobiotic sensor pxr and toll-like receptor 4," *Immunity*, vol. 41, no. 2, pp. 296-310, 2014.

[45] R. B. Bollipo, S. Mikkili, and P. K. Bonthagorla, "Critical review on pv mppt techniques: classical, intelligent and optimisation," *IET Renewable Power Generation*, vol. 14, no. 9, pp. 1413-1630, 2020.

[46] A. M. Bazzi and P. T. Krein, "Ripple Correlation Control: An Extremum Seeking Control Perspective for Real-Time Optimization," *IEEE Transactions on Power Electronics*, vol. 29, no. 2, pp. 988-995, 2014.

[47] P. T. Krein, "Ripple correlation control, with some applications," *1999 IEEE International Symposium on Circuits and Systems (ISCAS)*, vol. 5, pp. 283-286, 1999.

[48] A. Kopanicakova and G. E. Karniadakis, "Deeponet based preconditioning strategies for solving parametric linear systems of equations," *SIAM Journal on Scientific Computing*, vol. 47, no. 1, pp. C151-C181, 2025.

[49] M. Vidyasagar, *Nonlinear systems analysis*, SIAM, 2002.

[50] M. W. Spong, S. Hutchinson, and M. Vidyasagar, *Robot modeling and control*, John Wiley &amp, 2020.

[51] S. R. Islam, "Evaluation of Genetic Diversity among Mango (Mangifera indica L.) Hybrids and their Parentage using RAPD Markers," *Chemical Science Review and Letters*, vol. 7, no. 26, pp. 513-519, 2018.

[52] A. M. Eltamaly and M. A. Mohamed, "Optimal sizing and designing of hybrid renewable energy systems in smart grid applications," *Advances in renewable energies and power technologies*, vol. 2, pp. 231-313, 2018.

[53] K. Chafaa, L. Saidi, M. Ghanai, and K. Benmahammed, "Direct adaptive type-2 fuzzy control for nonlinear systems," *International Journal of Computational Intelligence and Applications*, vol. 6, no. 03, pp. 389–411, 2006.

[54] K. Chafaa, L. Saidi, M. Ghanai, and K. Benmahammed, "Indirect adaptive interval type-2 fuzzy control for nonlinear systems," *International Journal of Modelling, Identification and Control*, vol. 2, no. 2, pp. 106-119, 2007.

[55] S. Palomino-Resendiz, M. Penaloza-Lopez, D. Flores-Hern´andez, C. Solıs-Cervantes, and R. Palomino-Resendiz, "Model reference adaptive control (mrac) for dual-axis solar tracker applied in cpv," *Solar Energy Materials and Solar Cells*, vol. 279, p. 113225, 2025.

[56] B. Nishanthi and J. Kanakaraj, "Voltage stability assessment and power regulation of solar pv based dc microgrid," *Journal of Electrical Engineering & Technology*, vol. 20, no. 1, pp. 131-140, 2025.

[57] A. Zemmit *et al*., "GWO and WOA variable step mppt algorithms-based PV system output power optimization," *Scientific Reports*, vol. 15, no. 1, p. 7810, 2025.

[58] A. M. Malkawi *et al*., "Maximum power point tracking enhancement for pv in microgrids systems using dual artificial neural networks to estimate solar irradiance and temperature," *Results in Engineering*, vol. 25, p. 104275, 2025.

[59] V. Kevat, A. Sakhare, and S. Mikkili, "Design of non-isolated dc–dc converters for maximum power point tracking in stand-alone photovoltaic system," *Transactions of the Indian National Academy of Engineering*, vol. 10, pp. 191-221, 2025.

[60] M. F. Ali, M. R. I. Sheikh, A. A. Mamun, and M. J. Hossen, "Techno-Economic, Predictive Modeling, and Demand Response Analysis of a Renewable Energy-Based Microgrid for Residential Applications," *IEEE Access*, vol. 13, pp. 53748-53771, 2025.

[61] M. A. Ebrahim, A. M. El-Rifaie, B. A. Bahr, H. E. Keshta, M. N. Ali, and M. M. R. Ahmed, "Adaptive Control of a Hybrid Microgrid With Energy Storage System," *IEEE Open Journal of Power Electronics*, vol. 6, pp. 196-211, 2025.

[62] H. Karimi, A. Siadatan, and A. Rezaei-Zare, "A Hybrid P&O-Fuzzy-Based Maximum Power Point Tracking (MPPT) Algorithm for Photovoltaic Systems under Partial Shading Conditions," *IEEE Access*, 2025.

[63] L. Liu, "Photovoltaic mppt control and improvement strategies considering environmental factors: based on pid-type sliding mode control and improved grey wolf optimization," *Measurement and Control*, vol. 58, no. 2, pp. 227-244, 2025.

[64] P. Pathipooranam, "An enhanced efficient design of hybrid pv-teg system using improved dragonfly algorithm to extract maximum power under diverse operating circumstances," *SSRN*, 2025.